JOURNAL OF PROPULSION AND POWER
Vol. 8, No. 5, Sept.–Oct. 1992

Measured Particulate Behavior in a Subscale Solid Propellant Rocket Motor

W. D. Brennan,* D. L. Hovland,† and D. W. Netzer‡
Naval Postgraduate School, Monterey, California 93943

Particle size distributions were measured in the combustion chamber, exhaust nozzle, and exhaust plume of a small, two-dimensional rocket motor that utilized aluminized propellants. Various nozzle contours and pressures to 4.36 MPa were utilized. For pressures less than approximately 2.4 MPa, D_{32} of the multimodal size distributions entering the nozzle decreased with increasing pressure. Above 2.4 MPa, the higher propellant burning rates significantly reduced particle agglomeration and increased C^* efficiency. At higher pressures, D_{32} entering the nozzle was quite small (2–6 μ) and monomodal, and did not vary appreciably with pressure. During tailoff, D_{32} was significantly larger than during the steady burn, indicating another possible source for plume signature variations. Exhaust particle D_{32} was 1.2–1.6 μ (with a <2, 8, 28 μ trimodal distribution), independent of pressure, nozzle inlet contour, exit Mach number, degree of underexpansion, or location aft of the exit plane. The existence of a small number of larger particles indicated that either particle collision and/or surface effects occurred in the nozzle convergence, or that the larger particles at the nozzle entrance were concentrated near the wall, out of the viewing volume in the center of the flow.

Nomenclature

C^* = characteristic exhaust velocity
C_v = volume concentration of particles
D_{32} = Sauter mean diameter
d = particle diameter
I = intensity of transmitted light
I_0 = intensity of incident light
l = optical path length
M = Mach number
$N(d)$ = number of particles with diameters between d and $d + \Delta d$
P = pressure
Q = extinction coefficient
$\bar{Q}$ = average extinction coefficient for a distribution of particle sizes
Tr = transmittance, I/I_0
U = velocity
We = Weber number
α = mole fraction of oxidizing species
Δd = increment in particle diameter
ρ = density
σ = surface tension
τ = particle burning time

Subscripts
c = chamber
e = nozzle exit
g = gas
p = particle

Introduction

ALUMINUM is added to solid propellants to increase performance and to suppress high-freqency combustion instabilities. Most of the metal combustion is thought to occur in the gas phase, resulting in small[1] (<2 μ) metallic oxide particles. The burnout of larger aluminum agglomerates results in aluminum oxide particles typically >5 μ in diam. The two-phase flow losses and the exhaust plume signature can be effected by the particle size distribution. Codes such as the AFAL SPP[2] and OD3P[3] model the particulate behavior through the exhaust nozzle and estimate the resulting losses in performance. However, the particle sizes entering the nozzle are required as input data and the calculated behavior within the nozzle is semiempirical. Most often the codes are used with a value of D_{43}, which has been obtained from empirical data taken of collected exhaust products.[4] Very little is known about the actual behavior of the aluminum/aluminum oxide as it passes along the motor port and through the nozzle.[5]

A specific problem in the characterization of exhaust signature is the accurate prediction of particle breakup/agglomeration and particle trajectories within the exhaust nozzle and plume. Analytical models for these processes have not been validated adequately. Predictions of plume IR signature are sensitive to the specified initial conditions entering the nozzle, and the uncertainty in the size distributions and the degree to which gas/particle equilibrium assumptions are met are essentially unknown.[6] Some data[7] and the predictions of several models[8,9] indicate that the particle size distributions within an exhaust plume vary radially across the plume, with the larger particles concentrated along the plume centerline. This behavior could have a significant effect upon plume IR signature, depending upon the metal loading within the propellant.[10] Because Al_2O_3 particles act as scatterers, only small amounts of gas phase radiation can escape the plume when large amounts of particles are present. If there are a large number of very small particles in the outer regions of the plume, they may shield both gas-phase radiation and the radiation from the larger, hot particles. However, with reduced-smoke propellants that may have optically thin plumes, radiation can increase with particle mole fraction.[10] In this instance, particle size distribution can be very important. Data are needed on the effects of the cast powder size and composition, the initial particle size distribution entering the nozzle, the nozzle geometry, and the nozzle area ratio on the particulate processes and the exhaust particle size distribution. Plume structure (shocks, mixing, etc.) may also influence the particle size distribution.

In a recent effort,[11] a Malvern 2600HSD particle sizer was successfully used to measure the behavior of particulates within

Received Dec. 19, 1989; revision received Aug. 22, 1991; accepted for publication Nov. 30, 1991.

*Lieutenant, United States Navy, Graduate Student.
†Lieutenant Commander, United States Navy, Graduate Student.
‡Professor, Department of Aeronautics and Astronautics. Member AIAA.

the motor and exhaust nozzle of a small axisymmetric motor using a minimum smoke (ZrC) propellant. Difficulties with high obscurations through the motor at higher pressures and metal loadings resulted in the design and use of a small two-dimensional motor for the present investigation. The two-dimensional motor does introduce some undesirable conditions: heat loss through the side walls and nozzle geometries, which, without care, do not properly simulate axisymmetric nozzle flow. However, much needed information can be obtained under conditions that prevent collection of motor data.[5]

High obscurations can result in multiple scattering effects, which present difficulties when attempting to measure particle size distributions. Steering of the illuminating beam by density gradients in the particle-laden flow can also affect the particle measurements. Factors that may affect the particle size distribution inside the motor are many, including: percentage of metal in the propellant, metallic particle sizes in the unburned propellant, oxidizer particle size, combustion chamber pressure, burning rate of the propellant, and the residence time of the combustion products in the motor. It should be noted that mean residence time can be misleading when discussing expected particulate behavior. Particles entering the flow from the head-end of the grain port have sufficient time to burn to completion; whereas, particles leaving the aft end of the grain probably enter the nozzle flow as unburned aluminum. Exhaust particle size distributions may depend upon the above factors, as well as on the expansion process through the exhaust nozzle.

In an attempt to determine the impact of the expansion process on particle size, efforts to size particulate matter in the exhaust nozzle and exhaust plume were undertaken using both converging and converging-diverging nozzles of varying geometry in a small "two-dimensional" rocket motor. Particle sizing was accomplished at various chamber pressures using two different aluminum loadings (2 and 4.7%). Low metal loadings were chosen to minimize obscuration of the illuminating laser beam used for particle sizing. Although most aluminized propellants use higher metal loadings (10–20%), much can be learned about particulate behavior by observing flows with lower number densities of particles.[5]

Particle size distributions were measured using a Malvern 2600HSD. This instrument is based upon Fraunhofer diffraction in the near-forward direction. Use of the Malvern instrument for obtaining particle size distributions must be done with some care. In addition to beam steering, high obscurations result in multiple scattering. Empirical corrections exist,[12] or can be easily generated, for the mean properties like D_{32} and D_{43}, but the effect on the actual measured particle size distribution (location of mode peaks, etc.) needs to be determined. Another area that requires attention is the effect of the presence of particles that are outside the measurement range of the instrument on the "measured" particle size distribution.

Use of the Malvern 2600HSD for Measurements Within Rocket Motors

Motor Considerations

To prevent significant vignetting of the scattered light due to the required width of the motor, a 100-mm focal length Fourier transfer (focusing) lens was used, with a particle size range from 1.9–188 μ. The instrument also estimates the amount of particulate matter present between 0.5–1.9 μ. The instrument was operated in the model independent mode, which enables sizing of multimodal distributions. A 31-element, semicircular diode array is swept in 10 μs. However, processing time increases the "time/sweep" to approximately 7 ms. The number of sweeps taken in any experiment is a trade-off between statistical significance and the required time for data acquisition.

The 9-mm-diam He-Ne laser beam used in the Malvern presented some difficulties when used to measure the nozzle exit particle size distribution. The beam had to be placed upstream of the first Mach disk, but far enough downstream to prohibit the scattered light from striking the aft surface of the nozzle. Data at the exit plane where, therefore, taken with the beam positioned between 1.5 and 10.5 mm behind the motor.

Beam steering was observed within the exhaust plume of motor firings. This results in light impinging on the first few diode rings of the detector and prohibits the measurement of forward scattered light by the affected diodes. Approximately 84% of the diffracted energy from a particle lies within the first minimum of the Airy diffraction pattern. Eliminating the use of the inner eight diode rings of the array[13] that could be affected by beam steering would affect the above energy only for particles significantly larger than 30 μ in diam. Such large particles are not often observed in exhaust plumes.

Calibration/Validation Experiments

Polystyrene microspheres were obtained from the Duke Scientific Corporation. The particle distributions were of two types. The first was monomodal, with particle diameters varying several microns from the mode. These particles were documented with a histogram indicating the relative number of particles in each of approximately twenty size bands. These histograms were verified for several distributions by scanning electron microscope (SEM) photography. The second distribution type contained particles of a much more uniform size. These distributions were documented with a mean diameter and a standard deviation. The particles used in validation experiments were of both types and ranged in size from 0.109 to 20.0 μ.

Figure 1 show a plot of Malvern-measured D_{32} vs actual D_{32} for polystyrene spheres using the 100-mm lens. The results were excellent for D_{32} larger than 1 μ. For smaller particles, a D_{32} value of 0.9 μ is assigned.

With the prevalence of bimodal and trimodal distributions in past sizing experiments,[11] it was decided to evaluate the Malvern capability to handle such distributions using particles in liquid. SEM microscopy was also used to validate results further. Trimodal distribution experiments were conducted by first creating a trimodal mix from three known monomodal distributions of measured concentrations. D_{32} measured using the Malvern was compared to the value based upon the measured obscuration ($1 - Tr$), manufacturer-provided size distributions, and a calculated average extinction coefficient for the particles. For this purpose, Beer's law for a polydispersion[14] was utilized:

$$I/I_0 = \exp\left(\frac{-3\bar{Q}C_v l}{2D_{32}}\right) \tag{1}$$

For each monomodal distribution of polystyrene spheres, all values in the above expression except C_v were known or calculable. The manufacturer-provided size distribution, the mixture volume, and the measured volume concentration of particles were then sufficient to describe the distribution. The trimodal size distribution was then calculated by combining the three monomodal distributions.

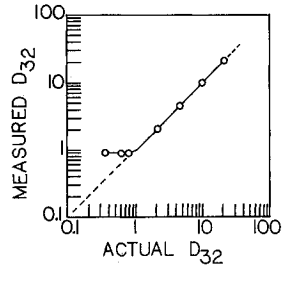

Fig. 1 Measured (Malvern) vs actual values of D_{32} for monomodal distributions.

Q for a given particle size was calculated from Mie theory, given the wavelength of the incident light and the complex refractive index of the particle (relative to the refractive index of the medium in which the particles were suspended). $\bar{Q}$ can then be calculated using[15]

$$\bar{Q} = \Sigma Q(d)N(d)d^2\Delta d/\Sigma N(d)d^2\Delta d \qquad (2)$$

The Miescat[16] code was modified to allow calculation of Q as a function of particle size and $\bar{Q}$ for a user-defined particle size distribution.

The trimodal mixture shown in Fig. 2 was created without violating either the dynamic range of the lens or the recommended obscuration limits. The Malvern-calculated D_{32} was less than the actual value. Multimodal distributions tended to reduce the calculated values of D_{32}, and did so in a repeatable fashion. Improper mixing of the particles could have affected the values of D_{32}, but would not have moved the mode peaks. The systematic underestimation of the diameters at mode peaks by 1–2 μ in trimodal distributions was consistently repeated, and resulted in underestimation of D_{32} for multimodal distributions. Nevertheless, the correct identification of the trimodal distribution type was most significant. In addition, for particles larger than approximately 3 μ, the measured accuracy of the mode peaks was better than the accuracy of D_{43} used in the SPP code.[4]

In similar experiments, Gulder[12] showed that for bimodal distributions, increased obscuration values tended to shift the calculated volume percentage of particles from the larger mode to the smaller mode. He showed that the Malvern measurements were correct for transmittance greater than 50% and presents an empirical correction for D_{32} values greater than 10 μ and transmittance between 2 and 50%.

Table 1 shows the effects of reducing the smallest mode size below the minimum measurable particle size. This models actual conditions in the two-dimensional motor. Mixture (a) contained a 0.624-μ mode. While below the minimum measurable particle size for the lens, the submicron particles clearly affected the measured D_{32}. These small particles were within the Malvern subclass of particles. The D_{32} values were close enough to be the result of experimental error, but the fact that the Malvern D_{32} was higher than the calculated value was significant. Had the Malvern been able to measure the submicron particles accurately, the Malvern generated D_{32} would have been lower than the actual value (due to the multimodal effects discussed above). Ignoring the submicron particles, the theoretical value of D_{32} for the remaining bimodal distribution was 15.5 μ. Thus, while the Malvern did not measure the "subclass" particles accurately, the results approximated the true distribution much more closely than an approximate distribution containing only the larger particles.

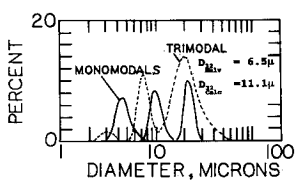

Fig. 2 Comparison of measured (Malvern) monomodal and trimodal volume distributions; all particles within instrument range and single particle scattering conditions.

Table 1 Measured and calculated values of D_{32} (μ)

	Calculated D_{32} for monomodal mixtures	Malvern-measured D_{32} for trimodal mixture	Calculated D_{32} for trimodal mixture
(a)	0.624[a,c]	2.4	1.9
	10.38		
	19.66		
(b)	0.511[a]	6.2	2.6
	5.33		
	9.83		
(c)	0.110[b]	6.6	0.16
	5.33		
	9.83		

[a]Below instrument measurement range but within subclass size.
[b]Significantly below instrument measurement range.
[c]High obscuration.

Mixtures (b) and (c) in Table 1 show results obtained using particles of approximately 0.5 μ and smaller. Such small particales were undetected by the Malvern in multimodal distributions. The effect was more pronounced when using the 0.109 μ particles in (c). The malvern D_{32} of 6.6 μ was what would have been expected for a multimodal mix if the smaller particles had not been present (calculated D_{32} = 7.4 μ). The Malvern value was slightly lower than 7.4 μ, as expected due to the multimodal effects on calculated D_{32} discussed above. Figure 3 shows the Malvern-generated volume distribution, that seems to be a bimodal distribution of the larger particles, with the largest mode located correctly and the center mode shifted to a smaller value. The Malvern did not detect the smaller particles. For such small particles, much of the scattered light misses the range lens, making a slightly higher obscuration the only discernable contribution to the light-scattering signature. Repeated experiments showed that if the smallest mode were comprised of 0.5 μ particles or smaller, it did not affect the measurements of the larger particles in a multimodal distribution. Table 2 shows the results for repeated measurements of a trimodal mixture consisting of 20.0, 9.6, and 4.8 μ particles, and reconfirmed the previously noted mode-dependent decrease in D_{32}.

Mix B in Table 2 was dehydrated and sized using a SEM. Comparison of SEM with calculated and Malvern measurements further validated the calibration method and confirmed that the Malvern locations for mode peaks were consistently small for trimodal distributions. It should be noted that, subsequent to this investigation, the latest Malvern software seems to have corrected this shift to smaller mode peaks.

Two-Dimensional Motor

The two-dimensional motor was designed by Pruitt[17] and Walker.[18] The internal dimensions were 5.8-cm-high × 0.64-cm-wide × 26.7-cm-long. Opposed slabs were burned with dimensions 0.64-cm-thick (optical axis) × 1.9-cm web (slabs were burned radially and on the nozzle end) × 7.6–21-cm length. The motor residence time was quite short, between 2–6 ms. This residence time is typical of small motors,[19] but results in significant amounts of unburned aluminum entering the exhaust nozzle together with the aluminum oxide. Nitrogen-purged windows were located within the motor port and at the nozzle inlet. The Malvern unit could be placed to measure through either window set or at the nozzle exit.

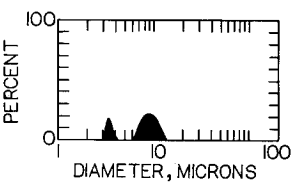

Fig. 3 Measured volume distribution for trimodal mix, Table 1(c).

Table 2 Results from monomodal and trimodal mixes

Particle distribution	Malvern D_{32}, μ	Calculated D_{32}, μ	SEM D_{32}, μ, 814 particle count
Monomodal 4.8 μ	4.3	4.73	—
Monomodal 9.6 μ	10.0	9.83	—
Monomodal 20.0 μ	21.8	21.91	—
Trimodal mix A	11.9	13.77	—
Trimodal mix B	12.3	13.77	13.53
Trimodal mix C	12.1	13.77	—

Several nozzle designs were utilized. Figure 4 shows one nozzle used to provide the same converging dA/dX as a 30 deg conical nozzle.[17] The throat size was 0.34 × 0.64 cm. Constant angle converging sections (Fig. 5) were also utilized. These nozzles had a throat area of 0.26 cm^2 and a 0.13-cm flat at the throat to minimize effects of throat erosion.

A simplified analysis was used to estimate the maximum expected particle sizes within the nozzle. Gas velocities were calculated using equilibrium gas properties from the propellant combustion, without particle drag effects. Particle velocities through the nozzles (as a function of size) were then calculated using the work of Caveny and Gany.[5] Weber number defined by

$$We = d_p\rho_g(u_g - U_p)^2/\sigma \qquad (3)$$

was then calculated. It was found that significant particle and gas accelerations were restricted to the throat region. Caveny and Gany[5] observed particle breakup for a critical Weber number of 28. However, Salita[3] reports an average value of approximately six is more appropriate. With this lower critical value, particles larger than approximately 8 μ were not expected at the throat.

Two converging-diverging nozzles with the medium length converging section and a 15 deg half-angle expansion were also used, producing ideal expansion for a combustion chamber pressure of either 1.03 MPa (exit $M \simeq 2.1$) or 3.45 MPa (exit $M \simeq 2.8$). Two GAP-AP propellants were utilized (Table 3).

Malvern and SEM analyses of the aluminum powder in these propellants resulted in a D_{32} of approximately 25 μ, with none larger than 60 μ.

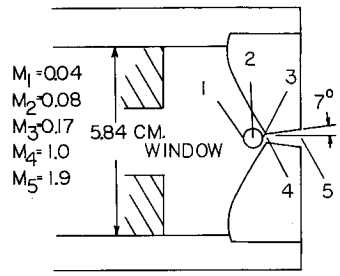

Fig. 4 Schematic of two-dimensional motor with measurement window location, simulated 30 deg conical converging nozzle section.

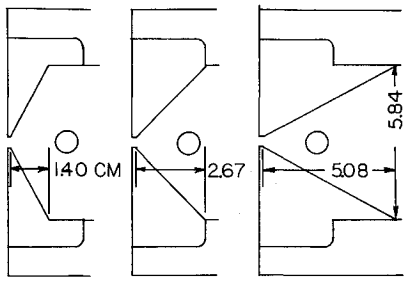

Fig. 5 Converging nozzle geometries.

Results and Discussion

Particles at the Nozzle Entrance

The data obtained either upstream of, or within, the converging nozzle are presented in Table 4 and Fig. 6. Data taken using the short converging nozzle were measured upstream of the nozzle. This data was used for the entrance conditions to the other nozzles since the throat areas and entering Mach numbers were the same. The converging-diverging nozzle used the medium length converging nozzle entrance, but it was offset from the windows. Thus, the data in the medium length converging nozzle could be displayed from multiple tests as shown in Fig. 7.

In Fig. 6 it is observed that the propellant with the lower aluminum content (2%) actually produced larger particles in the entrance section of the simulated conical nozzle at low pressures. This may have resulted from the 10% lower burning rate of the DD1 propellant compared to the DD5 propellant (1.14 vs 1.25 cm/s at 1.72 MPa). Measured values of D_{32} for the aluminum powder contained in the propellants varied between 24–29 μ. SEM analysis indicated that the largest particles were approximately 60 μ in diam. At motor pressures >2.4 MPa, most of the particles entering the nozzle were quite small (<5 μ). Figure 6 shows that, as expected,[20] the higher burning rates at higher pressures significantly reduced surface agglomeration. In addition, because D_{32} of the particles was significantly smaller than most of the particles cast into the propellant, the aluminum was apparently rapidly oxidized. The burning time of an aluminum agglomerate can be

Table 3 DD1 and DD5 propellant ingredients (wt%)

Ingredient	DD1	DD5
GAP	14.67	14.67
TEGDN	8.49	8.49
Aluminum	2.00	4.69
Tepanol	0.15	0.15
AP (200 μ)	47.45	45.70
AP (25 μ)	25.55	24.61
N-100	0.845	0.845
HDI	0.845	0.845

Table 4 Summary of nozzle entrance data

Propellant	Nozzle type	Chamber pressure, MPa	D_{32}, μ	Peaks of the volume distribution, μ
DD1	30 deg conical simulation	1.35	41	35, 48
		1.38	35	35, 48, 65
		1.65	33	25, 45, 65, 130 (weak)
		2.17	24	2.5, 35 (broad), 130 (weak)
DD5	30 deg conical simulation	1.14	22	3.2, 68 (broad)
		1.60	11	<2, 35, 70
		1.83[a]	13	2.2 (weak), 30, 50, 68, 130 (weak)
		2.40	1.8	2.8
		2.83[a]	10	2.8 (strong), 25, 130 (strong)
DD5	Short converging	2.47	3.7	<2, 15, 30
		2.73	3.3	3.3
		2.81	3.3	3.3
DD5	Medium converging	2.41	2.8	<2, 15, 30
		4.32	0.9	<2
DD5	Medium converging-diverging	2.77	1.5	2.5
DD5	Long converging	3.54	0.9	<2

[a]Data acquisition into tailoff.

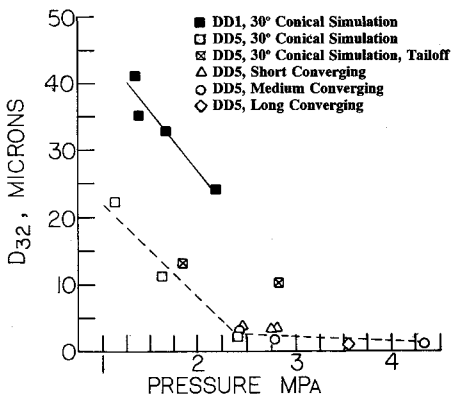

Fig. 6 Measured D_{32} at nozzle entrance.

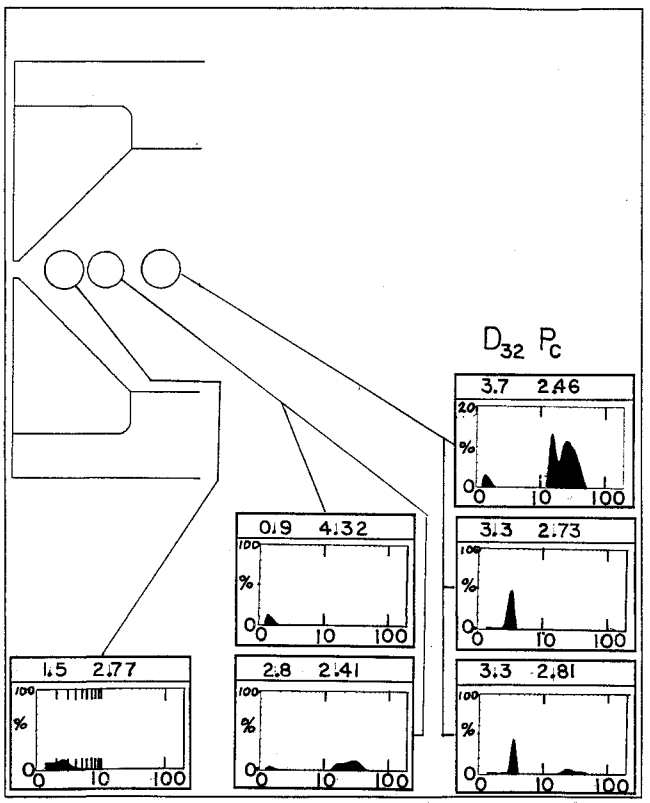

Fig. 7 Particle size volume distributions for 4.7% aluminized propellant (% in band vs diameter in μ), D_{32} in microns, P_c in MPa.

estimated from[20]

$$\tau = 7.3 \times 10^{-6} d_p^{1.75}/\alpha \qquad (4)$$

For the present investigation this time was approximately 2 ms for a 25-μ particle; roughly the same as the residence time of the motor. However, it should be cautioned that burning time does not associate directly with particle diameter due to the oxide shell formation process. D_{32} decreased with increasing pressure to pressures of approximately 2.4 MPa. Accurate calculations of C^* efficiencies were not possible due to the variations in propellant thickness. Small variations in the narrow thickness of the propellant resulted in inaccurate knowledge of the burning surface area. However, for the DD5 propellant at pressures less than 2.4 MPa, the C^* efficiency averaged approximately 10% less than for higher pressures. Thus, the larger mean particle sizes at lower pressures correlated with the combustor performance. Figure 7 shows that for a pressure near 2.7 MPa, some particle size reduction occurred in the converging section of the nozzle (3.3 → 2.8 → 1.5 μ). These particles are much smaller than would be expected to break up due to exceeding a critical Weber number of even six.

Another interesting result is seen in Fig. 6. When the data sampling time included some of the tailoff pressure, D_{32} was significantly increased. During tailoff pressure drop, when the total number density of particles is decreasing, the quantity of larger particles may actually increase. This could result in significant changes in plume radiation during tailoff, in addition to the expected increase in soot radiation that results from liner and inhibitor charring.

The data in Table 4 for the DD5 propellant indicated that, not only did D_{32} change with pressure, but also the shape of the particle size distribution. Except for very low pressures (1.14 MPa) the particles were typically trimodal to 2.4 MPa and monomodal for higher pressures. As pressure was increased, fewer of the larger agglomerates were present and more of the smaller (<2 μ) particles were present.

Particles in the Exhaust Plume

The data obtained in the exhausts from the nozzles are presented in Table 5 and Fig. 8. The DD1 propellant (2% Al) had larger particles in the exhaust than the DD5 (4.7% Al) propellant for pressures less than approximately 3.8 MPa. This followed the behavior observed for the nozzle inlet conditions. One plausible explanation for this behavior is that when larger particles break up, they do so to yield particles smaller than would be calculated from a critical Weber number; the smaller the initial size, the smaller the resulting size. Once the particles are smaller than the critical size for the nozzle throat, they would not change further in size except for agglomeration and/or condensation effects. The above result was obtained for the simulated conical entrance geometry with an exit Mach number of 1.9; all data with $P_c >$ 0.69 MPa were for underexpanded nozzle flow conditions. For this nozzle, with the DD1 propellant, the exhaust distributions were quadramodal with peaks in the distribution at approximately <2, 5, 15, and 25 μ. Most of the particles were <2 μ in size, but a significant amount of the mass (volume distribution) was contained in the small number of larger particles. The existence of these larger particles can be important for plume radiation and as ignition sources for afterburning.

Considering the DD5 propellant (where most of the particles entering the nozzles were typically <20 μ in size), the particle D_{32} was typically 1.2–1.6 μ, independent of nozzle inlet contour, exit Mach number, degree of underexpansion, or location aft of the exit plane. Shocks in the plume apparently had no effect on the particles, indicating that the very small particles probably were in a solid state due possibly in part to high gas cooling rates to the two-dimensional motor walls. Most of the distributions were quadramodal or trimodal, with a few particles greater than 20 μ passing through the throat region into the plume.

At higher pressures, the particles entering the nozzle were small (<4 μ) and monomodal; whereas, downstream of the throat they were trimodal, with small numbers of particles having mean diameters of approximately 8 and 28 μ. This indicated that particle collisions and/or surface impingement-shedding occurred, or that the larger particles were concentrated near the walls of the converging nozzle out of view of the centrally located windows.

Probe Data

The AFAL particle collection probe[21] was also used with the DD1 propellant in an initial attempt to compare collected particulate data with the nonintrusive optical data. A low-pressure (0.83 MPa) test was conducted in order to provide near-ideal expansion condition for the simulated conical nozzle. Laser sheet and video recordings were used on earlier tests to ensure that no shocks would be present in the plume. In addition, the probe was placed 4.17-cm aft of the exhaust

Table 5 Summary of nozzle exit data

Propellant	Nozzle type	Chamber pressure, MPa	D_{32}, μ	Peaks of the volume distribution, μ
DD1	30 deg conical simulation, M_e = 1.9, $P_e = P_a$ @ P_c = 0.69 MPa	0.83[b]	3.7	
		0.90	3.3	<2, 5.5 (weak), 12, 15
		1.43	2.7	<2, 15, 25
		2.32	2.8	<2, 5.5, 11, 25
		3.70	2.0	<2, 5.5 (weak), 17, 25
DD5	30 deg conical simulation, M_e = 1.9, $P_e = P_a$ @ P_c = 0.69 MPa	0.99	1.8	<2, 6.5 (weak), 16, 26
		1.60	1.5	<2, 15, 26
		2.44	1.7	<2, 6.5, 16, 25
		3.92	1.7	<2, 6.5, 16, 25
DD5	Medium length converging, $P_e = P_{critical}$	1.99	1.3	<2, 8, 28
		2.10	1.2	"
		2.28[a]	0.9	"
		2.34	1.4	"
DD5	Long length converging, $P_e = P_{critical}$	1.43	1.4	<2, 8, 28
		1.63	1.4	"
		1.69	1.5	"
		1.97	1.3	"
		2.18	1.4	"
DD5	Medium length converging-diverging, M_e = 2.1, $P_e = P_a$ @ P_c = 1.03 MPa	2.69[a]	1.3	<2, 8, 28
		3.30[a]	1.2	<2, 8
		4.16	1.3	<2, 8, 28 (weak)
DD5	Medium length converging-diverging, M_e = 2.8, $P_e = P_a$ @ P_c = 3.45 MPa	2.94	1.6	<2, 7, 29
		3.38[a]	1.6	"
		3.61[a]	1.5	"

[a]Data taken further aft in plume.
[b]Particle collection probe data.

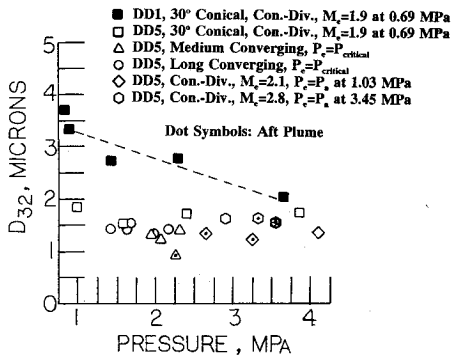

Fig. 8 Measured D_{32} in exhaust plume.

plane in order to meet the probe design requirement for swallowing approximtely 1 gm/s. No attempt was made to eliminate ignition or tailoff particles. The entire burn time was 3.2 s. SEM analysis of the particles caught on the filter paper showed spherical particles between <0.5 μ and 9 μ in diam. 773 particles were counted with a D_{32} of 3.7 μ. This was in good agreement with the optical measurements made at 0.90 MPa, where D_{32} was 3.3 μ.

Summary and Conclusions

The Malvern 2600HSD particle sizer used in the model independent mode was found to be reasonably accurate for use in the solid propellant rocket motor environment. High obscurations in the motor and nozzle entrance regions can limit its application to determination of qualitative particulate behavior. In the exhaust plume, beam steering of the laser occurred, but was not a significant problem due to the small (<30 μ) particles that were present.

Investigations utilizing polystyrene spheres showed that the Malvern instrument was quite accurate for characterizing monomodal distributions. It also correctly indicated the presence of multimodal distributions, but underestimated the diameters of the peaks of the smaller modes—in the 2–10 μ range. No corrections for multiple scattering were found necessary for obscurations less than 50%. Particles smaller than 0.5 μ were found not to influence the measured distributions of larger particles.

For pressures less than approximately 2.4 MPa, D_{32} of the multimodal size distributions entering the nozzle decreased with increasing pressure. Above 2.4 MPa, the higher propellant burning rates significantly reduced particle agglomeration. This was also evident from higher C^* efficiency for pressures above 2.4 MPa. Above 2.4 MPa, the mean particle size entering the nozzle was quite small (on the order of 2–6 μ) and did not vary appreciably with pressure. This indicated that rapid aluminum oxidation occurred within the motor. At higher pressures (>2.76 MPa) the distributions became monomodal in the center of the flow at the nozzle entrance.

The mean particle size D_{32} entering the nozzle during motor tailoff was significantly larger than during the steady burn, indicating an additional source for plume signature variations during tailoff.

For a 2% aluminized propellant, larger particles entering the nozzle were found to result in larger plume particles for pressures less than approximately 3.8 MPa. Exhaust particle size distributions were generally quadramodal for this propellant, with most of the particles less than 2 μ in diam, but with significant mass (volume) contained in a small number of larger (6–30 μ) particles.

Exhaust particle D_{32} for a 4.7% aluminum propellant was 1.2–1.6 μ (with a <2, 8, and 28 μ trimodal distribution), independent of entering particle size, pressure, nozzle inlet contour, exit Mach number, degree of underexpansion, or location aft of the exit plane. In contrast, the particles entering the nozzle at higher pressures were typically monomodal, with none of the larger particles present. This indicated that particle collision and/or surface impingement-shedding occurred, or that the larger particles were concentrated near the walls of the converging nozzle, out of view of the centrally located windows.

To pressures of 4.14 MPa, particles larger than expected from a critical Weber number behavior were measured in the exhaust plume.

An initial use of the AFAL particle collection probe at low motor pressure showed particle sizes in good agreement with the optical data.

Acknowledgment

This investigation was supported by the Air Force Astronautics Laboratory, Edwards Air Force Base, California under MIPR R0461189X0006.

References

[1]Salita, M., "Quench Bomb Investigation of Al_2O_3 Formation from Solid Rocket Propellants (Part II): Analysis of Data," *Twenty-fifth JANNAF Combustion Meeting*, Vol. 1, Chemical Propulsion Information Agency Publication 498, Oct. 1988, pp. 185–197.

[2]George, D., "Recent Advances in Solid Rocket Motor Performance Prediction Capability," AIAA Paper 81-033, *Nineteenth Aerospace Sciences Meeting*, St. Louis, MO, Jan. 1981.

[3]Salita, M., "Implementation and Validation of the One-Dimensional Gas/Particle Flow Code OD3P," *Twenty-sixth JANNAF Combustion Meeting*, Oct. 23–27, 1989.

[4]Hermsen, R. W., "Aluminum Oxide Particle Size for Solid Rocket Motor Performance Prediction," AIAA Paper 81-035, *Nineteenth Aerospace Sciences Meeting*, St. Louis, MO, Jan. 1981.

[5]Caveny, L. H., and Gany, A., "Breakup of Al/Al_2O_3 Agglomerates in Accelerating Flow Fields," AIAA Paper 79-0300, *Seventeenth Aerospace Sciences Meeting*, New Orleans, LA, Jan. 1979.

[6]Dash, S. M., Pearce, B. E., Pergament, H. S., and Fishburne, E. S., "Prediction of Rocket Plume Flowfields for Infrared Signature Studies," *Journal of Spacecraft and Rockets*, Vol. 17, No. 3, 1980, pp. 190–199.

[7]Fewell, K. P., and Kessel, P. A., "Analysis, Design, and Testing of Components of a Combined Ablation/Erosion Nozzle," Arnold Engineering Development Center TR 75-154, March 1976.

[8]Dash, S. M., "Analysis of Exhaust Plumes," *Tactical Missile Aerodynamics*, Vol. 104, Progress in Astronautics and Aeronautics, AIAA, New York, 1986, pp. 778–851.

[9]Hwang, C. J., and Chang, G. C., "Numerical Study of Gas-Particle Flow in a Solid Rocket Nozzle," *AIAA Journal*, Vol. 26, No. 6, 1988, pp. 682–689.

[10]Nelson, H. F., "Influence of Particulates on Infrared Emission from Tactical Rocket Exhausts," *Journal of Spacecraft and Rockets*, Vol. 21, No. 5, 1984, pp. 425–432.

[11]Youngbourg, E. E., Pruitt, T. E., Smith, M. J., and Netzer, D. W., "Light Diffraction Particle Size Measurements in Small Solid Propellant Rockets," *Journal of Propulsion and Power*, Vol. 26, No. 3, 1990, pp. 243–249.

[12]Gulder, O. L., "Multiple Scattering Effects in Drop Sizing of Dense Fuel Sprays by Laser Diffraction," *AGARD Seventeenth Symposium of the Propulsion and Energetics Panel on Combustion and Fuels in Gas Turbines*, Oct. 1987.

[13]Koo, J. H., "Particle Size Analysis Using Integral Transform Techniques on Fraunhofer Diffraction Patterns," Ph.D. Thesis, George Washington Univ., Washington, DC, April 1987.

[14]Dobbins, R. A., Crocco, L., and Glassman, I., "Measurements of Mean Particle Sizes of Sprays from Diffractively Scattered Light," *AIAA Journal*, Vol. 1, No. 8, 1963, pp. 1881–1886.

[15]Cashdollar, K. L., Lee, C. K., and Singer, J. M., "Three-Wavelength Light Transmission Technique to Measure Smoke Particle Size and Concentration," *Applied Optics*, Vol. 18, No. 11, Washington, DC, 1979, pp. 1763–1769.

[16]Cashdollar, K. L., "Miescat," Fortran Computer Program, 1976.

[17]Pruitt, T. E., "Measurements of Particle Size Distributions in a Solid Propellant Rocket Motor Using Light Scattering," Master's Thesis, Naval Postgraduate School, Monterey, CA, June 1987.

[18]Walker, J. D., "Holographic Investigation of Metallized Solid Propellant Combustion in Two Dimensional and Three Dimensional Rocket Motors," Master's Thesis, Naval Postgraduate School, Monterey, CA, Sept. 1987.

[19]"Solid Propellant Selection and Characterization," NASA SP-08064, June 1971.

[20]Price, E. W., "Combustion of Metalized Propellants," *Fundamentals of Solid-Propellant Combustion*," Vol. 90, Progress in Astronautics and Aeronautics, AIAA, New York, pp. 479–513.

[21]Misener, J. A., and Kessel, P. A., "Current AFRPL Measurements and Characterization of Particulates in Solid Rocket Motor Plumes," *Fifteenth JANNAF Plume Technology Meeting*, May 1985.